Experimental study of the reactions $e^+e^- \to e^+e^-$ and $e^+e^- \to \gamma\gamma$ at 29 GeV

M. Derrick, K. K. Gan,[a] P. Kooijman, J. S. Loos,[b] B. Musgrave, L. E. Price, J. Schlereth, K. Sugano, J. M. Weiss,[c] and D. E. Wood[d]
Argonne National Laboratory, Argonne, Illinois 60439

D. Blockus, B. Brabson, S. W. Gray,[e] C. Jung, H. Neal, H. Ogren, D. R. Rust, and M. Valdata-Nappi[f]
Indiana University, Bloomington, Indiana 47405

C. Akerlof, G. Bonvicini, J. Chapman, D. Errede, N. Harnew,[g] P. Kesten,[h] D. I. Meyer, D. Nitz, A. A. Seidl,[d] R. Thun, T. Trinko,[d] and M. Willutzky
University of Michigan, Ann Arbor, Michigan 48109

S. Abachi, P. Baringer, I. Beltrami,[i] B. G. Bylsma, R. DeBonte, D. Koltick, F. J. Loeffler, E. H. Low, U. Mallik,[a] R. L. McIlwain, D. H. Miller, C. R. Ng, L. K. Rangan,[d] and E. I. Shibata
Purdue University, W. Lafayette, Indiana 47907

B. Cork
Lawrence Berkeley Laboratory, Berkeley, California 94720
(Received 12 May 1986)

This paper reports measurements of the differential cross sections for the reactions $e^+e^- \to e^+e^-$ (Bhabha scattering) and $e^+e^- \to \gamma\gamma$ (γ-pair production). The reactions are studied at a center-of-mass energy of 29 GeV and in the polar-angular region $|\cos\theta| < 0.55$. A direct cross-section comparison between these two reactions provides a sensitive test of the predictions of quantum electrodynamics (QED) to order α^3. When the ratio of γ-pair to Bhabha experimental cross sections, integrated over $|\cos\theta| < 0.55$, is divided by the same ratio predicted from α^3 QED theory, the result is $1.007 \pm 0.009 \pm 0.008$. The 95%-confidence limits on the QED-cutoff parameters are $\Lambda_+ > 154$ GeV and $\Lambda_- > 220$ GeV for Bhabha scattering, and $\Lambda_+ > 59$ GeV and $\Lambda_- > 59$ GeV for γ-pair production.

I. INTRODUCTION

The reactions

$$e^+e^- \to e^+e^- \quad \text{(Bhabha scattering)} \tag{1}$$

and

$$e^+e^- \to \gamma\gamma \quad (\gamma\text{-pair production}) \tag{2}$$

have been the subject of much recent experimental study[1-7] in the energy region from 29 to 45 GeV covered by the colliding-beam facilities PEP at SLAC and PETRA at DESY. These fundamental reactions provide a sensitive means of testing for unexpected departures from quantum electrodynamics (QED) at small distances. No significant differences from QED have been reported, aside from small electroweak [Glashow-Salam-Weinberg (GSW)] effects[8] that affect Bhabha scattering by a few percent at these energies. These reactions can therefore be used to set limits on QED-cutoff parameters,[9,10] or to search for new phenomena, such as the effects of composite models[11] or high-mass spin-zero bosons that couple to e^+e^- (Ref. 12).

This paper reports results from a high-statistics study of these reactions carried out with the High Resolution Spectrometer (HRS) at the PEP e^+e^- storage-ring facility. The measurements are made in the central polar-angle region $|\cos\theta| < 0.55$, and are based on an integrated luminosity of 165 pb^{-1} collected at a center-of-mass energy of 29 GeV. The statistical precision and the control of systematic uncertainties are improved over previous work on these reactions. A particular emphasis of the present work is to reduce systematic uncertainties so that the two reactions can be compared directly to one another as a test of α^3 QED theory.[13] The principal findings of the present analysis have already been published in final form;[14] this paper completes the discussion of event selections, corrections, and analysis methods, and provides tables of differential cross sections for these reactions.

The lowest-order differential cross section for Bhabha scattering is given by

$$(d\sigma^0_{ee}/d\Omega)_{\rm GSW} = (\alpha^2/2s)[\,|A_1|^2(s/t)^2 + |A_2|^2(t/s)^2 + \tfrac{1}{2}(|A_3|^2 + |A_4|^2)(1+t/s)^2\,], \tag{3}$$

where $s = E_{\text{c.m.}}^2$, $t = -s(1-\cos\theta)/2$, and θ is the scattering angle. For energies well below the mass of the Z^0 boson, the electroweak amplitudes are

$$\begin{aligned} A_1 &= 1+(g_V^2-g_A^2)\chi(t) , \\ A_2 &= 1+(g_V^2-g_A^2)\chi(s) , \\ A_3 &= 1+s/t+(g_V-g_A)^2[\chi(s)+(s/t)\chi(t)] , \\ A_4 &= 1+s/t+(g_V+g_A)^2[\chi(s)+(s/t)\chi(t)] , \end{aligned} \tag{4}$$

where

$$\chi(q^2) = \frac{G_F}{\pi\alpha\sqrt{8}} \frac{q^2 M_Z^2}{(q^2-M_Z^2)} .$$

In these expressions, G_F is the Fermi coupling constant, α is the fine-structure constant, M_Z is the mass of the Z^0, g_V is the vector coupling, and g_A is the axial-vector coupling. If the electroweak contributions are ignored by setting $g_A = g_V = 0$, then the pure-QED expression for Bhabha scattering in lowest order is

$$(d\sigma_{ee}^0/d\Omega)_{\text{QED}} = (\alpha^2/4s)(3+\cos^2\theta)^2/(1-\cos\theta)^2 . \tag{5}$$

At 29 GeV, the electroweak effect reduces the pure-QED differential cross section by only 1–2% (Refs. 15–17).

The lowest-order differential cross section for γ-pair production is given by

$$(d\sigma_{\gamma\gamma}^0/d\Omega)_{\text{QED}} = (\alpha^2/s)(1+\cos^2\theta)/\sin^2\theta . \tag{6}$$

Electroweak contributions for this reaction can occur only in high-order diagrams and are negligible at the present energy.

Deviations from the QED predictions are usually expressed in terms of cutoff parameters $\Lambda_\pm$. For Bhabha scattering, small cutoff terms[9] are added to the amplitudes of Eq. (4):

$$\begin{aligned} A_1' &= A_1 \pm t/\Lambda_\pm^2 , \\ A_2' &= A_2 \pm s/\Lambda_\pm^2 , \\ A_3' &= A_3 \pm 2s/\Lambda_\pm^2 , \\ A_4' &= A_4 \pm 2s/\Lambda_\pm^2 . \end{aligned} \tag{7}$$

For truly pointlike scattering the Λ are infinite. For Bhabha scattering, the principal contribution from the cutoff terms is through interference with the main terms. To a good approximation, the ratio of differential cross sections with and without the cutoff terms is

$$(d\sigma_{ee}/d\Omega)/(d\sigma_{ee}/d\Omega)_{\text{QED}} = 1 \mp (3s/\Lambda_\pm^2)\sin^2\theta/(3+\cos^2\theta) . \tag{8}$$

For γ-pair production, the cutoff terms do not interfere with the main terms and the result is usually parametrized[10] in the form

$$(d\sigma_{\gamma\gamma}/d\Omega)/(d\sigma_{\gamma\gamma}/d\Omega)_{\text{QED}} = 1 \pm (s^2/2\Lambda_\pm^4)\sin^2\theta . \tag{9}$$

The plan of the paper is as follows. A brief review of th HRS detector characteristics and the experimental running is given in Sec. II. Detailed discussions of the event selections and corrections for reactions (1) and (2), respectively, are presented in Secs. III and IV. Section V is devoted to α^3 QED calculations and the simulation of the experiment. The final results for the differential cross sections and QED cutoff parameters are presented in Sec. VI. A brief summary is given in Sec. VII.

II. APPARATUS AND EXPERIMENTAL RUNNING

A. The High Resolution Spectrometer

Detailed descriptions of the detector systems and the performance of the High Resolution Spectrometer (HRS) appear elsewhere in the literature,[1,18,19] so only a brief outline will be repeated here. The elements of the HRS,

TABLE I. List of detectors and material in the High Resolution Spectrometer

Radius (cm)	Detector (or material)	Thickness (r.l.)	Coverage in cos θ	Comments
7.6	Ti foil	0.0015		
7.6	Be beam pipe	0.0040		
8.6–13.3	Vertex detector	0.0051	−0.9–0.9	Four-layer, axial drift tubes.
15.3	Be pipe	0.0025		Inner wall of central DC.
21–103	Central drift chamber (DC)	0.009	−0.9–0.9	2448 cells arranged in seven axial layers and eight stereo layers (±60 mr).
112–114	Al hexcell	0.005		Outer wall of central DC.
120–180	Cherenkov centers	0.25	−0.65–0.65	Threshold counters in pressure vessels.
186–192	Outer drift chamber	0.06	−0.66–0.66	896 axial drift tubes in two layers.
195–220	Barrel calorimeter	11	−0.61–0.61	Pb scintillator and proportional wire tubes.
65–160	End-cap calorimeter	11	−0.94–(−0.75) 0.75–0.94	Pb scintillator and proportional wire tubes.

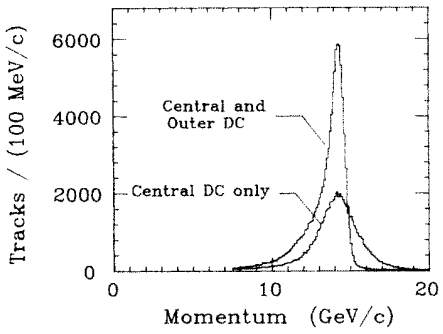

FIG. 1. Momentum distributions of e^+ and e^- tracks from Bhabha scattering in the HRS. The beam energy is 14.5 GeV, and the tracks are restricted to the central polar-angle region $|\cos\theta| < 0.55$. The narrow distribution is found for tracks measured to their full potential length, whereas the wide distribution is found for tracks measured only over the region of the central drift chamber.

listed in Table I, are all located within the large solenoidal magnet field volume (4.45 m diameter and 4.0 m in length). The central magnetic field is 1.62 T, and there is a variation of only $\sim 5\%$ over the tracking volume. The detectors used in the present work are the central and outer drift chambers and the barrel calorimeters.

Track-finding and first-stage reconstruction of particle trajectories are done with algorithms that examine only the information from the central drift chamber. Tracks successfully reconstructed in the central chamber are then extrapolated to the outer drift tubes to seek matching hits, and (if found) the reconstruction is repeated in order to improve the momentum measurement. Additional track-reconstruction steps, including a vertex constraint and/or information from the vertex chambers are available, but are not used in the present work.

The excellent momentum resolution achieved with the HRS is illustrated in Fig. 1, which shows the distribution of measured momenta of e^+ and e^- particles from Bhabha scattering. The resolutions in momentum and production angles for these particles are summarized in Table II. The momentum resolution is degraded by a factor of ~ 4.3 when the outer drift-chamber measurements are unavailable; this is the case for 38% of the electrons, which tend to radiate in the Cherenkov pressure vessels. However, as seen in Fig. 1, the quality of tracks measured only by the central drift chamber is still good enough that a clean momentum cut can be applied in selecting Bhabha events.

TABLE II. Resolution for e^+ and e^- tracks in the HRS detector. These resolutions are for track reconstruction without using a vertex constraint or any information from the vertex chamber.

Tracking variable	Resolution
Azimuth	$\sigma_\phi = 2.2$ mrad
Polar angle	$\sigma_\theta = 6.5$ mrad
Momentum (setting error)	$\sigma_{p_T}/p_T = 0.0017 p_T$[a]
(p_T in GeV/c)	$= 0.0075 p_T$[b]
Momentum (multiple scattering)	$\sigma_{p_T}/p_T = 0.0055$

[a]Track reconstructed using both the central and outer drift chambers.
[b]Track reconstructed using the central drift chamber only.

The total thickness of material from the beam line to the middle layer of the central drift chamber is only 0.017 radiation lengths (r.l.). This thin front end and the good momentum resolution are important for obtaining a thorough understanding of certain systematic effects, such as photon conversions, event identification ambiguities, and tracking problems that can affect electrons.

The barrel calorimeter system is essential in the study of these reactions. Table III gives a synopsis of the characteristics of the system for energetic showers. A detailed discussion of the performance of this system is given in Ref. 19. Photon shower positions are normally determined by a combination of proportional-wire-chamber (PWC) measurements and timing measurements from both ends of the barrel. A small fraction (4.3%) of the photons convert beyond the PWC plane; these showers are located with adequate resolution using only the mea-

TABLE III. Summary of characteristics of the HRS barrel calorimeter system for measuring energetic showers.

Number of modules in system	40
Detector arrangement	Pb-scintillator sandwich (3 r.l.); 14 PWC tubes/module with charge division; Pb-scintillator sandwich (8 r.l.); 4 photomultipliers/module
Angular coverage of one module	9° in azimuth and $-0.61 < \cos\theta < 0.61$
Energy resolution	$(\sigma_E/E)^2 = (0.16)^2/E + (0.06)^2 + (0.011)^2 E$ (E in GeV)
Timing resolution	$\sigma_t = 185$ psec for showers
Azimuthal-angle resolution	$\sigma_\phi = 7.4$ mrad (with PWC) $= 60$ mrad (without PWC)
Polar-angle resolution	$\sigma_\theta = 8$ mrad (PWC and timing) $= 12$ mrad (timing alone)

surements from the scintillators. The simple geometry and polar symmetry of the barrel system are well matched to the drift chambers, and are also important in understanding the detector calibrations and in reducing possible polar asymmetries or other systematic effects.

The HRS proved to be stable and reliable in operation. The fraction of inoperative drift-chamber cells during experimental running was typically less than 1%; these dead cells were scattered randomly in the chambers and caused no significant tracking losses. The barrel calorimeter system operated with virtually no downtime. The end-to-end redundancy of the barrel system was valuable in maintaining high efficiency, since signals could be missing at one end (because of a failed photomultiplier or base) without seriously degrading the shower information. Care was taken to monitor minor problems (e.g., power supply failures, gas flow rates) that could affect either experimental triggers or recorded data; such problems occurred in fewer than 1% of the experimental runs and these runs were rejected for analysis.

B. Data sample and integrated luminosity

The data were collected during a two-year running period at a center-of-mass energy of 29 GeV. There were no significant detector modifications during this period. The integrated luminosity of the data sample was independently measured by the wide-angle events from both reactions (1) and (2), as summarized in Table IV. The weighted average value is 164.8 pb^{-1}. The measurements given in Table IV are discussed in detail later in this paper.

C. Event triggering

All candidate events were required to satisfy just one hardware trigger based on the energy deposited in the barrel system. For this trigger, a portion of the analog photomultiplier signals from all barrel modules were summed in a fast network. If this sum exceeded the equivalent of 4.8 GeV, then an event trigger was generated, regardless of any other information from the event. Events from these reactions normally deposited nearly 29 GeV in the barrel. All such events were recorded on tape, and became candidates for reactions (1) and (2). Requiring this single hardware trigger avoided potential systematic differences between the two reactions, since they produce nearly identical signals in the barrel system. Moreover, any undetected failure of the barrel system would affect both reactions equally.

A statistical check of the event triggering is summarized in Table V. The γ-pair events are expected to occur in random sequence within the combined sample of events from these reactions. A failure of the drift-chamber tracking could cause Bhabha events to be misclassified as γ pairs; any lengthy failure of this type would yield a number of consecutive false γ-pair events. Table V gives the distribution in the grouping of consecutive γ pairs observed in the final data sample. The data are in excellent agreement with the numbers computed assuming that the two reactions occur in random sequence. Thus there is no evidence of any tracking failures that could cause misclassification between these reactions.

TABLE IV. Integrated luminosity measured in this analysis.

Reaction	$e^+e^- \to e^+e^-$	$e^+e^- \to \gamma\gamma$
Integrated luminosity	164.4 pb^{-1}	165.6 pb^{-1}
Statistical uncertainty	0.4%	0.8%
Systematic uncertainty	0.5%	0.6%
Weighted average[a]	164.8(1±0.006) pb^{-1}	

[a]The systematic uncertainty arising from the α^3 QED calculations is not included, and is estimated to be in the range of 1%.

TABLE V. Distribution of consecutive γ-pair events in the combined final sample of γ-pair and Bhabha events.

N	Number of groups of N consecutive γ-pair events: Observed	Expected
1	10766	10766.0
2	1656	1597.9
3	212	232.2
4	36	40.3
5	2	6.6
6	1	1.0
>6	0	1.2

D. Check of azimuthal uniformity of the HRS

In the polar region used, $|\cos\theta| < 0.55$, the tracking system is uniform and crack-free. This uniformity is demonstrated in Fig. 2, which displays the distribution of track azimuth for e^+ and e^- tracks from the final sample of Bhabha events. The distribution is flat, as expected for a uniform detector and unpolarized beams. Since the azimuths of the two particles are correlated, the proper statistical test of flatness is to average over all sets of 90 adjacent bins of 2°. This yields $\chi^2 = 92.0$ for 89 degrees of freedom.

The barrel calorimeters are also uniform in azimuth, except for the mechanical walls between modules. The shower energy leakage in these walls affects a few percent

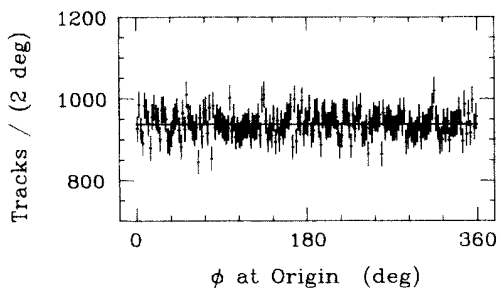

FIG. 2. Distribution in production azimuth for e^+ and e^- tracks from Bhabha scattering. The distribution is expected to be flat for a uniform tracking system and unpolarized e^+e^- colliding beams.

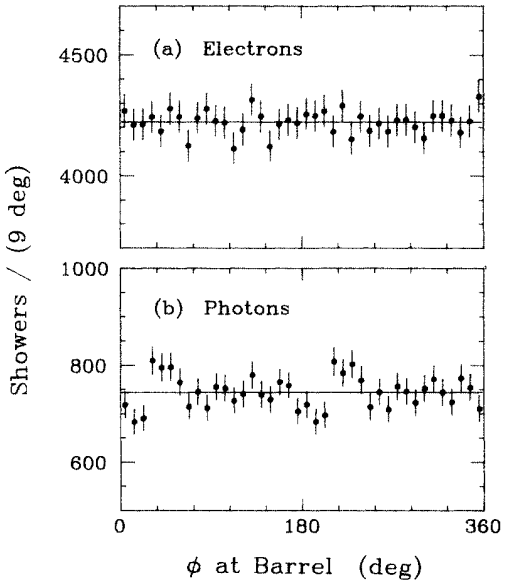

FIG. 3. Distribution in azimuth projected to the HRS barrel calorimeter for (a) e^+ and e^- particles from Bhabha scattering, and (b) photons from γ-pair production. Each bin of 9° matches the size of one barrel module in order to emphasize possible differences among modules. The distributions are expected to be flat for a uniform calorimeter system and unpolarized e^+e^- colliding beams.

of the events (see discussions in Secs. III and IV). The module-to-module uniformity of the barrel is demonstrated by displaying the azimuthal distribution of the showers observed at the barrel in 9° bins (one bin per module). This is done for the final sample of Bhabha events in Fig. 3(a), and for the final sample of γ-pair events in Fig. 3(b). Both distributions are consistent with being flat. Averaging over all sets of 20 adjacent bins gives $\chi^2=10.8$ for 19 degrees of freedom for the Bhabha sample, and $\chi^2=30.9$ for 19 degrees of freedom for the γ pairs.

III. EVENT SELECTIONS AND CORRECTIONS FOR THE REACTION $e^+e^-\to e^+e^-$

A. Event selections

All events satisfying the hardware energy trigger were passed through the track- and shower-reconstruction programs. Candidate Bhabha events were then required to satisfy all of the following preliminary criteria: (a) one, two, three, or four reconstructed tracks; (b) $E>3.0$ GeV for two (or more) showers; (c) $|\cos\theta|<0.6$ for two (or more) showers; (d) acollinearity <0.25 rad between any pair of showers or between any two tracks having $p>7.5$ GeV/c. The acollinearity angle between two unit vectors, $\hat{\mathbf{u}}$ and $\hat{\mathbf{v}}$, is defined as $\arccos(-\hat{\mathbf{u}}\cdot\hat{\mathbf{v}})$. These preliminary selections retain candidates that have a knock-on electron, an externally converted radiative photon, a missing track, or a spurious track(s).

Events were included in the final sample of Bhabha events if they passed all of the following stricter "standard" cuts: (a') momentum cut, $p>7.5$ GeV/c for exactly two tracks of opposite charge; (b') energy cut, $E>3.75$ GeV in the barrel for two showers matched to the tracks; (c') fiducial cut, $|\cos\theta|<0.55$ for both charged tracks; (d') acollinearity cut, acollinearity <0.20 rad between the charged tracks; (e') time cut, times of flight within ±2.5 nsec of the expected arrival time. Note that radiative final states are allowed by these cuts.

A small fraction of legitimate events passed (a)—(d), but for a variety of reasons did not pass (a')—(e'). To find these events, all of the one-, three-, and four-track candidates, as well as those two-track events that had a substandard track reconstruction, were examined in detail by a physicist. Approximately 5000 events were examined. Legitimate events (i.e., those which would have passed the standard cuts if no tracking problem had occurred) recovered by this process are included in the final Bhabha event sample.

B. Observed events

The classifications and the final numbers of observed events are given in Table VI. There are 81 992 events (97%) that passed the standard cuts, and 2431 events (3%) that were recovered by the physicist scan. Most of the recovered events have two visible tracks, all have at least one satisfactorily reconstructed track, and all have two legitimate showers that are matched to the tracks. Because of the thin front end of the HRS, only about 0.5% of the events have tracks coming from knock-on electrons or external photon conversions. The recovered events have been corrected by removing spurious tracks, or by inferring the energy and direction of missing tracks from a matching calorimeter shower. This method of event identification accounts for every candidate, and therefore it is systematically more reliable than methods that estimate event losses on the basis of Monte Carlo simulation of detector performance.

C. Corrections and uncertainties

Table VII summarizes the corrections to the Bhabha sample. Some of the entries depend upon calculations of α^3 QED theory and a detailed simulation of the experiment discussed later. Each correction and its systematic uncertainty are discussed below in some detail.

1. Higher-order QED events and $e^+e^-\gamma$ events with an external photon conversion

Higher-order QED processes can produce four-track events (or three-track events with one track missing) that satisfy (a')—(e') for two of the tracks. This background is small and easily removed in the present experiment, as shown in Fig. 4. This plot is a distribution of the "kissing radius" for the lowest-energy e^+e^- combination from the four-prong candidates. The kissing radius is the distance between the origin and the point of closest approach of the two tracks in the plane transverse to the beam; its sign is negative if this point lies in the hemisphere opposite to the momentum direction of the pair. A small signal of

TABLE VI. Observed Bhabha event sample.

Number of tracks reconstructed	Number of events	Category
1	682[a]	Two tracks visible, one track fails to reconstruct.
2	81 992	Satisfies standard selections.
	199[a]	One track incorrectly reconstructed with wrong sign of curvature.
	430[a]	One track has too few measured points and is falsely reconstructed.
3	70	Third track is a knock-on electron.
	177	Third track is from an asymmetric external photon conversion.
	503	Spurious track removed; two good tracks remain.
	146[a]	Two spurious tracks reconstructed instead of one real track.
4	183	Two tracks from external photon conversion; satisfies Bhabha selections.
	41	Two spurious tracks removed, two good tracks remain.
Observed event total	84 423	

[a]Direction of missing track determined from matching shower in the barrel calorimeter.

higher-order QED events (mainly $e^+e^- \to e^+e^-e^+e^-$) is evident at zero kissing radius. These events are almost entirely removed by requiring the kissing radius to exceed 4 cm. This simple cut is effective because the kissing radius for externally converted photons follows closely the known distribution of material in the HRS (see Table I). The resolution in the kissing radius is of the order of 1 cm for the converted photons, as demonstrated by the prominent peaks seen at the radius of the beam pipe and at the radius of the inner wall of the central drift chamber.

The three- and four-track events accepted into the final Bhabha sample are presumed to be predominantly $e^+e^-\gamma$ final states. This assumption has been checked by a plot of the pair momentum k, shown in Fig. 5. The shaded events are three-track events for which the missing track is visible, but not reconstructed; for these events, the momentum of the missing track has been estimated by hand measurement. The distribution agrees well with the expected $1/k$ distribution shown by the curve. The events with $k \lesssim 0.4$ GeV are classified as standard Bhabha events because neither of the low-energy tracks is reconstructed. The $1/k$ spectrum also becomes depleted at momenta

TABLE VII. Corrections and systematic uncertainties for the Bhabha sample.

Effect	Correction
Ambiguities from higher-order QED processes or misidentification of legitimate $e^+e^-\gamma$ events	(0.0±0.1)%
Backgrounds from cosmic-ray showers, beam-gas collisions, hadronic annihilations, or $\tau^+\tau^-$ pairs	<0.1%
Loss at azimuthal structures between barrel modules	(2.1±0.2)%
Bremsstrahlung[a]	(0.0±0.3)%
Fiducial, acollinearity, and momentum cuts	(0.0±0.2)%
Observed event total: 84 423	
Corrected event total: 86 190	
Statistical uncertainty: 0.4%	
Systematic uncertainty: 0.5%	

[a]Hard external bremsstrahlung reduces the momentum acceptance by 2.7%; internal bremsstrahlung reduces it by an additional 1.3%. These effects are corrected in the Monte Carlo simulation of the experiment.

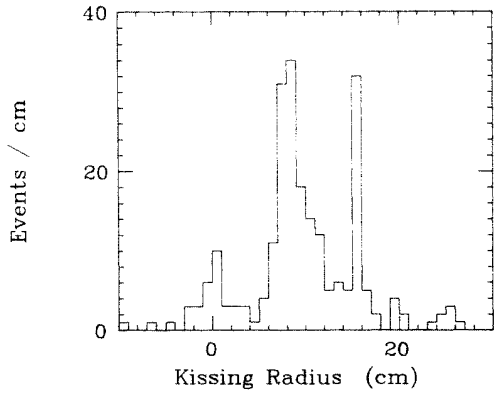

FIG. 4. Distribution of kissing radius of the lowest-energy e^+e^- combination for events appearing to be from the reaction $e^+e^- \to e^+e^-e^+e^-$. The kissing radius is a measure of the apparent vertex position of the pair of tracks. The events having a kissing radius larger than about 4 cm are $e^+e^-\gamma$ final states for which the photon converts externally in the material of the tracking region; most of these events satisfy the Bhabha selection criteria.

above ~ 5 GeV; this is expected as a result of the cuts (a')—(d'). An additional check on the efficiency of finding the converted pairs is shown in Fig. 6, which is a distribution of energy partition between the e^+ and e^- tracks. The data are in good agreement with the theoretical result averaged over the photon energy range.[20] This plot also shows that the three-track events arise mainly from asymmetric photon conversions.

The systematic uncertainty caused by ambiguities with higher-order QED events (including $\gamma\gamma$ interactions) and by misidentification of legitimate $e^+e^-\gamma$ final states with an externally converted photon is estimated to be at 0.1%.

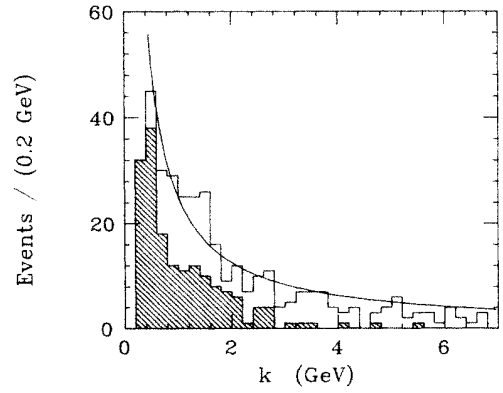

FIG. 5. Observed momentum distribution of the photon from the sample of $e^+e^-\gamma$ final states having an externally converted photon. The unshaded events have four reconstructed tracks. The shaded events have three reconstructed tracks, and a fourth visible track that has been measured by hand. The spectrum is observed to be consistent with the expected $1/k$ shape (curve), where k is the pair energy.

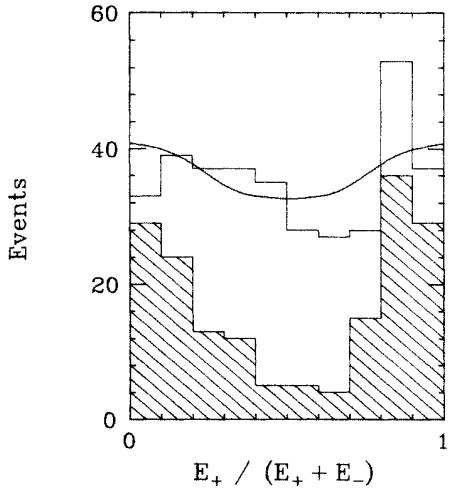

FIG. 6. Distribution of energy partition between the e^+ and e^- tracks from the converted pairs of Fig. 5. The shading here has the same meaning. The curve is the theoretical prediction.

2. Backgrounds

The combined background from the following sources is less than 0.1%:

(a) Cosmic-ray events. A total of 15 cosmic-ray showers passed the loose cuts (a)—(d). These events were examined in the physicist scan; all failed the timing cut (e') and most also failed the momentum cut (a').

(b) Beam-gas collisions. These events, which tend to have low energy and to be quite acollinear, are effectively eliminated by the standard cuts (a')—(d'). It is estimated that there are fewer than five such events in the final sample.

(c) Hadronic annihilation. Based on a study of the multiplicity distributions in this experiment,[21] the number of two-prong hadronic events within the fiducial cut (c') is 25 ± 25. The momentum and energy cuts, (a') and (b'), would reduce the number by at least a factor of 10. Therefore, this background is estimated to be no more than five events.

(d) $e^+e^- \to \tau^+\tau^-$. Approximately 7500 τ pairs are produced within the fiducial cut. The decays, $\tau^\pm \to e^\pm \nu\bar{\nu}$ and $\tau \to$ charged hadron plus neutrals, can occasionally satisfy the Bhabha selections. The known branching ratios, together with an approximate model of the decay distributions, yield a background from this source of 50 events, or 0.06%.

3. Event loss at the azimuthal walls between the barrel modules

If one of the Bhabha electrons enters the barrel calorimeter near an azimuthal wall between modules, then the shower energy leakage may be so large that the event fails to satisfy the energy requirement (b'). This effect is shown in Fig. 7(a), which displays the distribution of electron azimuth projected to the barrel. The azimuth is plotted modulo 9° in order to add and align the distributions from all 40 modules. A small loss is observed near the

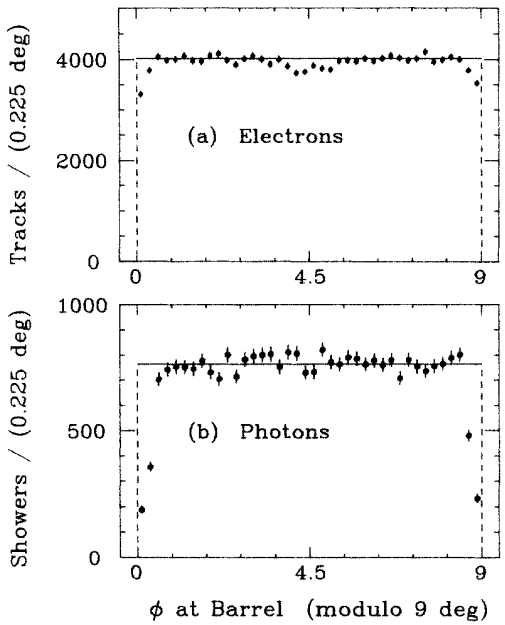

FIG. 7. Distribution in azimuth, modulo 9°, projected to the barrel calorimeter for (a) e^+ and e^- particles from Bhabha scattering, and (b) photons from γ-pair production. This plot adds and aligns the distributions from all 40 barrel modules in order to display the event losses caused by shower leakage near the azimuthal walls of the modules.

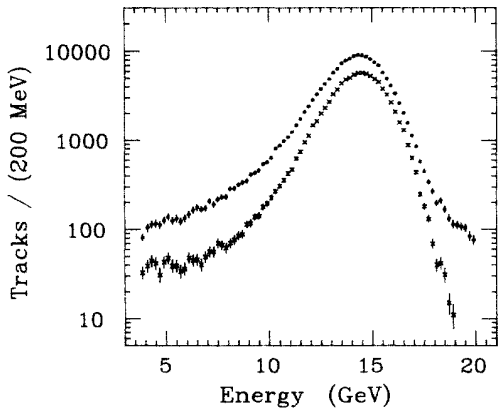

FIG. 8. Spectrum of barrel shower energy of e^+ and e^- particles from Bhabha scattering. The upper plot (solid points) shows all tracks, whereas the lower plot (crosses) shows a subset chosen to avoid shower leakage at the walls of the barrel modules (see the text).

module walls. The dip near the center of the distribution is a reflection of this edge loss (if one track enters near a module edge, then the other track is magnetically deflected so that it enters the barrel near the center of a module). The loss amounts to (2.1±0.2)% of the Bhabha signal. It is independent of polar angle; thus this correction applies only to the cross section, and not to the angular distribution.

The distribution of shower energy for electrons from accepted Bhabha events is shown in Fig. 8. The upper distribution shows all tracks, whereas the lower one displays the subset of tracks that have a momentum between 13 and 16 GeV/c and an azimuth (projected to the struck barrel module) between 1° and 8°. A comparison between the two distributions indicates that very few Bhabha events are removed by cut (b'), except for those with a track entering the barrel near a module wall. Since this effect has already been taken into account, no further correction is necessary.

4. *Effect of bremsstrahlung on momentum acceptance*

The measured momentum distribution of the e^+ and e^- particles for the accepted Bhabha events is shown in Fig. 9(a) together with the expected distribution (histogram), which has been calculated with α^3 QED theory, smeared by detector resolution, and corrected for the effect of bremsstrahlung. For comparison, Fig. 9(b) shows the same data and the same calculated distribution, but with the bremsstrahlung correction turned off. The bremsstrahlung clearly shifts a portion of the observed spectrum to lower momenta; if this shift were ignored, then a systematic error in the momentum acceptance would be introduced by the momentum cut at 7.5 GeV/c. This error could be large for detectors that have substantial material in the tracking region. The curve in Fig. 9(a), which reproduces the data well, corresponds to a correction to the cross section of (4.0±0.3)%. This

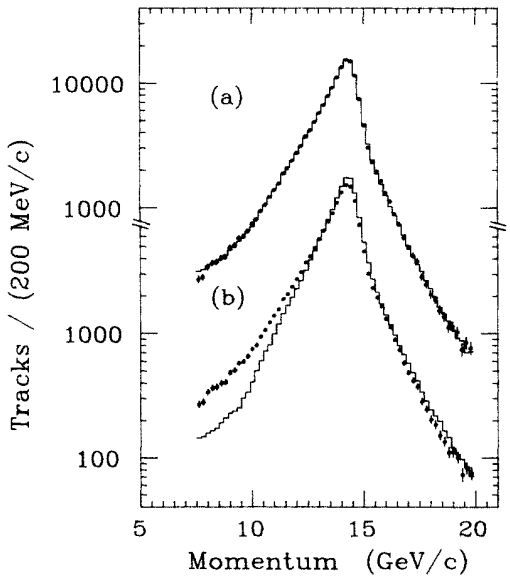

FIG. 9. Momentum distribution of e^+ and e^- particles from Bhabha scattering. (a) shows the data (solid points) together with the prediction of the full α^3 QED Monte Carlo simulation of the experiment (histogram). (b) shows the same data compared to a similar simulation that has neglected the effects of bremsstrahlung (see the text).

correction consists of two pieces: 2.7% from external bremsstrahlung in the material of the HRS and 1.3% from an estimate of the effect of α^4 QED terms ("internal" bremsstrahlung) that are ignored in the α^3 QED calculation. The quoted error in the correction is an estimate of the systematic contributions in the calculation. The 4.0% correction is applied in the Monte Carlo simulation of the experiment.

5. *Uncertainty caused by event selections*

The cross section should be independent of the data selections applied for momentum, acollinearity, and fiducial region because the same cuts are also used in the Monte Carlo simulation (from which the cross section is derived). However, if the simulation of the experiment is not sufficiently accurate, then the ratio of observed to simulated events will be unstable when these cuts are varied, leading to a systematic error in the measurement of the cross section.

The stability of the Bhabha cross section is excellent when these cuts are varied, as is summarized in Table VIII. Since the variations caused by the three cuts are nearly independent, they have been added in quadrature to yield the systematic uncertainty of 0.2% listed in Table VII. The stability of the momentum cut is illustrated in Fig. 9(a), where the calculated distribution reproduces the data over the whole momentum range. The stability of the acollinearity cut is similarly illustrated in Fig. 10, where the acollinearity distribution for the Bhabha sample is compared to the Monte Carlo simulation.

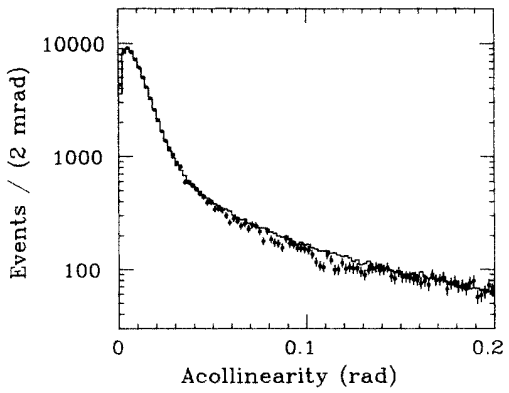

FIG. 10. Distribution in acollinearity for Bhabha scattering. The solid points are data and the histogram is the prediction of the full α^3 QED Monte Carlo simulation of the experiment.

IV. EVENT SELECTIONS AND CORRECTIONS FOR THE REACTION $e^+e^- \to \gamma\gamma$

The γ-pair reaction has been studied in parallel with the Bhabha reaction, using similar techniques in order to reduce the relative systematic uncertainties. Although the γ-pair events have no tracks, the signals in the barrel calorimeter are almost the same for the two reactions.

A. Event selections

Events that passed the hardware energy trigger were retained for study if all of the following were satisfied: (a) 0, 1, or 2 reconstructed tracks; (b) $E > 3.0$ GeV for two (or more) showers; (c) $|\cos\theta| < 0.6$ for two (or more) showers; (d) acollinearity < 0.25 rad between any pair of showers. These selections include events having one externally converted photon. They also keep events from the $\gamma\gamma\gamma$ final state.

Events in the final sample of γ pairs were required to pass all of the following tighter "standard" cuts: (a')

TABLE VIII. Number of Bhabha events observed for various event selection criteria. The ratios of observed to expected events are determined by applying identical cuts to the data and to the Monte Carlo simulation of the experiment.

Selection criteria used				
Track momentum (GeV/c)	Acollinearity angle (rad)	Fiducial region $\lvert\cos\theta\rvert$	Number of observed events	Ratio $\left[\frac{\text{observed}}{\text{expected}}\right]$
>7.5[a]	<0.20[a]	<0.55[a]	84 423	1[b]
>8.0	<0.20	<0.55	83 689	1.0011
>8.5	<0.20	<0.55	82 779	1.0015
>9.0	<0.20	<0.55	81 740	1.0021
>9.5	<0.20	<0.55	80 395	1.0015
>7.5	<0.22	<0.55	84 977	0.9993
>7.5	<0.18	<0.55	83 721	0.9999
>7.5	<0.16	<0.55	82 915	1.0004
>7.5	<0.14	<0.55	82 001	1.0011
>7.5	<0.20	<0.57	91 061	0.9980
>7.5	<0.20	<0.56	87 632	0.9987
>7.5	<0.20	<0.54	81 163	0.9986
>7.5	<0.20	<0.53	78 153	0.9986

[a]Standard value for data selection.

[b]The ratio is defined to be unity for the standard selections.

track cut, no track coming from the origin; (b′) energy cut, $E > 3.0$ GeV for (at least) two showers; (c′) fiducial cut, $|\cos\theta| < 0.55$ for the showers satisfying (b′); (d′) acollinearity cut, acollinearity < 0.20 rad between any pair of showers satisfying both (b′) and (c′); (e′) timing cut, times of flight within ± 2.5 nsec of the expected arrival time.

In order to find legitimate γ-pair events having one or two tracks from an externally converted photon, a physicist scan was done for all one- and two-track events that passed (a)—(d) but that did not pass the Bhabha selections. Also included in the scan were all zero-prong events that passed (a)—(d) but that had a substandard shower reconstruction, or that had more than 13 struck drift-chamber cells, or that had three or more clearly separated showers. The zero-prong scan determined the background level from cosmic-ray showers, searched for Bhabha events with failed tracks that might be misclassified as γ pairs, confirmed legitimate events with substandard showers, and located legitimate $\gamma\gamma\gamma$ final states. Approximately 1500 events were examined. Events recovered by this process are included in the final sample, provided that they would have passed the standard cuts if no photon had converted or if no confusion in shower reconstruction had occurred.

B. Observed events

Table IX lists the final numbers of observed events. There are 14 410 zero-prong events (97%) that satisfied the standard cuts; of these, 403 have a substandard shower reconstruction but were certified by the physicist scan, and another 174 were identified as $\gamma\gamma\gamma$ final states that passed the criteria (a′)—(e′). The remaining events in the final sample (3%) have an externally converted photon, and are distributed among several categories. The energies and shower positions of some of the recovered events have been corrected by hand correlation of tracking and shower information. As was the case with the Bhabha sample, all candidate events are accounted for with the present method. No uncertainties are introduced by simulating the efficiency of shower reconstruction or by simulating the detector efficiency for identifying converted photons.

A cross-check on the amount of material in the HRS tracking region (see Table I) is provided by the number of observed γ-pair events with a converted photon. A total of 365 events have a photon conversion in the beam pipe, vertex chamber, or inner wall of the central drift chamber whereas 325 such events are expected from the material listed in Table I. The agreement is reasonable, although the observed number is 2 standard deviations higher than the calculated number. This suggests that the amount of material in Table I may be underestimated by 0.0017 ± 0.0008 r.l. An error in material thickness of this magnitude would have no effect on the γ-pair sample, and would also have a negligible affect on the Bhabha results.

C. Corrections and uncertainties

The corrections to the γ-pair sample are summarized in Table X. Some of the entries depend upon α^3 QED calculations and the simulation of the experiment discussed later. Each correction and its systematic uncertainty are discussed below.

TABLE IX. Observed γ-pair event sample.

Number of tracks reconstructed	Number of events	Category
0	13 833	Satisfies standard selections.
	403	Confused or substandard shower present; event certified by physicist scan.
	174	Identified by scan to be $\gamma\gamma\gamma$ event; satisfies $\gamma\gamma$ selection criteria.
1	7	Photon converts in beam pipe or walls; one track fails to reconstruct.
	26	Photon converts in drift chamber gas volume; one track fails to reconstruct.
2	358	Photon converts in beam pipe or walls.
	66	Photon converts in drift-chamber gas volume.
	13	Identified by scan o be $\gamma\gamma\gamma$ event, where the softest photon convertes externally; satisfies $\gamma\gamma$ selection criteria.
Observed event total	14 880	

TABLE X. Corrections and systematic uncertainties for the γ-pair sample.

Effect	Correction
Unusable legitimate events or ambiguities from higher-order QED processes	(0.2±0.3)%
Backgrounds from cosmic-ray showers or hadronic annihilations	<0.1%
Loss at azimuthal structures between barrel modules	(5.9±0.4)%
Fiducial and acollinearity cuts	(0.0±0.3)%
Observed event total: 14 880	
Corrected event total: 15 850	
Statistical uncertainty: 0.8%	
Systematic uncertainty: 0.6%	

1. Ambiguous events and unusable legitimate events

Figure 11 shows the distribution of kissing radius for the candidates with tracks. Pairs in this plot are required to have an invariant mass less than 600 MeV/c^2. For the small subsample of shaded events, the second track was hand measured because it failed to reconstruct. The track pairs in Fig. 11 usually have energies near the beam energy, and have a resolution in kissing radius of 2–3 cm. There is a clear signal of events that have tracks produced at the origin. These do not belong to the γ-pair sample; rather, they are predominantly $e^+e^-\gamma$ final states for which the photon emerges with nearly the full beam energy and the charged particles have a low effective mass. These events also do not belong to the Bhabha sample because they fail the acollinearity requirement. These events are removed by requiring the kissing radius to exceed 4 cm. The uncertainty introduced into the γ-pair sample by this cut is estimated to be ±30 events.

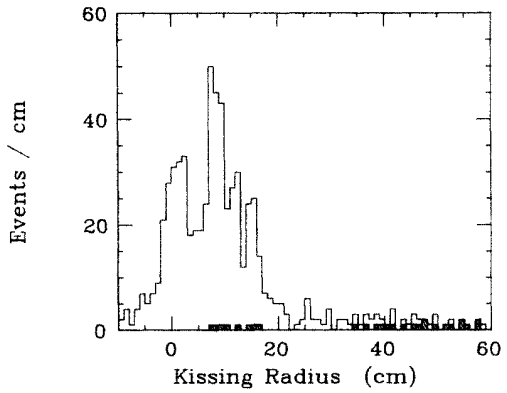

FIG. 11. Distribution of kissing radius of the γ-pair candidates that appear to have one converted photon. The unshaded events have two reconstructed tracks, whereas the shaded events have one reconstructed track and a second visible track that has been hand measured. The events having a kissing radius larger than 4 cm are considered legitimate γ-pair events if all other selections are satisfied (see the text).

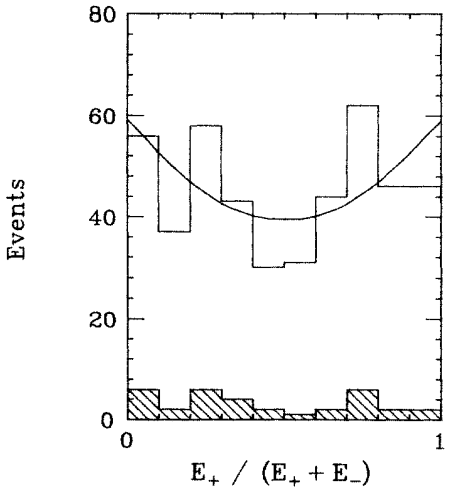

FIG. 12. Distribution of energy partition between the e^+ and e^- tracks from the converted pairs of Fig. 11. The curve is the theoretical prediction.

The distribution of energy partition between the e^+ and e^- tracks for the externally converted pairs is shown in Fig. 12. The observed distribution is consistent with the expected distribution,[20] but could allow a small loss of ~10 events with asymmetric pairs.

The physicist scan found a small number of γ pairs that were omitted from the sample, including six apparently legitimate zero-prong events that cannot be used because they have poor shower information, and an estimated 18 events from the one- and two-track samples that have unusable tracking information. From these studies, it is estimated that a correction of (0.2±0.3)% accounts for the ambiguous and unusable events.

2. Backgrounds

There were 328 cosmic-ray showers that passed the loose cuts (a)–(d), and were examined in the physicist scan. All of them failed the timing cut (e') by at least 5 nsec and most also had visible tracks that obviously did not come from the origin. In the scan of zero-prong events with 13 or more struck drift-chamber cells, only three Bhabha events were found with both tracks failing, so this is a negligible background. Backgrounds from beam-gas collisions, $\gamma\gamma$ interactions, and hadronic annihilations also appear to be negligible. The total background is therefore estimated to be less than 0.1%.

3. Event loss at the azimuthal walls between the barrel modules

As with the Bhabha sample, there is a loss of signal when a photon enters the barrel calorimeter near one of the azimuthal walls between the modules. This is shown in Fig. 7(b), which displays the distribution of photon azimuth modulo 9°. The distribution is flat, except near the walls, where the signal loss is determined to be (5.9±0.4)%. This loss is independent of polar angle. This

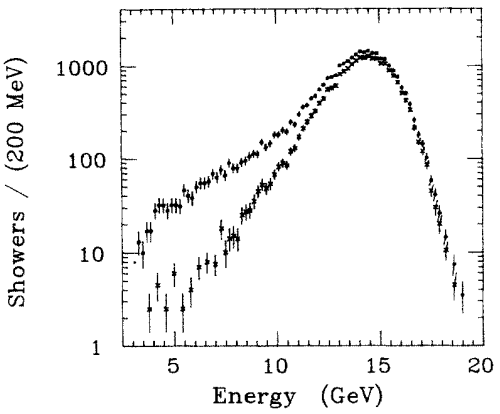

FIG. 13. Spectrum of barrel shower energy for the photons from γ-pair production. The upper plot (solid points) shows all photons, whereas the lower plot (crosses) shows a subset chosen to avoid shower leakage at the walls of the barrel modules (see the text).

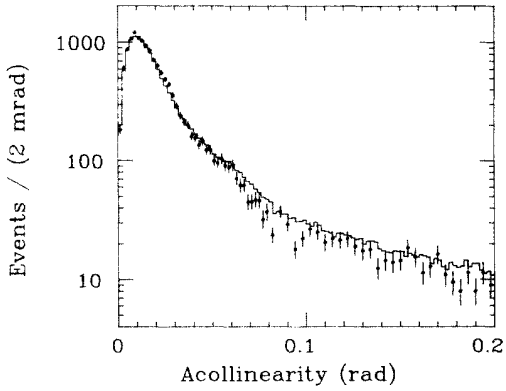

FIG. 14. Distribution in acollinearity for γ-pair production. The solid points are data and the histogram is the prediction of the full α^3 QED Monte Carlo simulation of the experiment.

effect is smaller for Bhabha events than for γ pairs because the electron tracks are deflected by the magnetic field and tend to intersect at least part of a Pb-scintillator sandwich.

The distribution of shower energy for photons from the final event sample is shown in Fig. 13, where the upper distribution is for all photons and the lower one is for the subset of photons that enter the barrel modules with an azimuth between 1° and 8°. As expected, the low-energy tail is predominantly from photons entering the barrel near the module walls. No correction for the energy cut (b') is needed beyond that already applied.

4. Uncertainty caused by event selections

The γ-pair cross section is quite stable against variations in the event-selection criteria, as shown in Table XI. The systematic uncertainty in the cross section associated with these cuts is estimated to be 0.3%. The acollinearity distribution for the γ-pair events, shown in Fig. 14, is in excellent agreement with the Monte Carlo simulation.

V. QED THEORY TO ORDER α^3 AND SIMULATION OF THE EXPERIMENT

In order to make detailed comparisons of QED theory to experiment, a large sample of numerically generated events is needed. These events are smeared according to experimental conditions, and then subjected to the same cuts as were applied to the data. For the present analysis, the ratio of simulated events to observed events was about 10. This section outlines the steps used in this procedure.

A. QED calculations

The QED calculations were done using the program of Berends and Kleiss,[13] which use Monte Carlo techniques

TABLE XI. Numbers of γ-pair events observed for various selection criteria. The ratios of observed to expected events are determined by applying identical cuts to the data and to the Monte Carlo simulation of the experiment.

Selection criteria used			Ratio
Acollinearity angle (rad)	Fiducial region $\lvert\cos\theta\rvert$	Number of observed events	$\left[\frac{\text{observed}}{\text{expected}}\right]$
<0.20[a]	<0.55[a]	14 880	1[b]
<0.22	<0.55	14 985	1.0035
<0.18	<0.55	14 788	1.0038
<0.16	<0.55	14 666	0.9992
<0.14	<0.55	14 512	0.9978
<0.20	<0.57	15 800	0.9996
<0.20	<0.56	15 362	1.0023
<0.20	<0.54	14 458	1.0038
<0.20	<0.53	14 039	1.0048

[a]Standard value for data selection.
[b]The ratio is defined as unity for the standard selections.

to generate events in the (elastic) final states, e^+e^- and $\gamma\gamma$, and in the radiative final states, $e^+e^-\gamma$ and $\gamma\gamma\gamma$. The calculations are complete to order α^3, and therefore include the lowest-order diagrams, virtual diagrams, and diagrams leading to a single radiated photon. For Bhabha scattering, the virtual effects arise from self-energy and box diagrams, from vertex corrections, and from vacuum polarization. Only the vertex and box diagrams contribute to the virtual corrections for γ-pair production. Infrared divergence is avoided by combining the elastic and radiation diagrams in the soft-photon approximation. The cutoff is chosen such that photons from radiative events satisfy $k/E_{\text{beam}} > 0.01$, where k is the photon energy.

The calculations of Berends and Kleiss proceed as follows. First, it is decided whether a trial event will be radiative or elastic; this is determined from the ratio of radiative and elastic cross sections. Next, the vectors for the final-state particles are chosen (by suitable Monte Carlo methods) on the basis of the theoretical differential cross sections. Then, an event weight is computed from the probability for finding that particular final-state configuration. Finally, the generated event is randomly accepted into (or rejected from) the final sample of theory events according to this weight, such that the accepted events all have unit weight. The programs do careful bookkeeping so that the total cross section (to order α^3) is computed for the phase space in which the events are generated.

The Bhabha scattering simulation was done with the electroweak contribution turned off. At 29 GeV, this contribution is only 1–2 % of the Bhabha differential cross section. It is included later in the analysis by a separate calculation. Electroweak effects are entirely negligible in γ-pair production, since there are no low-order diagrams involving annihilation through a single photon.

B. Experiment simulation for Bhabha scattering

For a generated elastic Bhabha event, an extrapolation procedure is used to add soft photons to the energy region below the soft-photon cutoff. If the event is not elastic, then it is corrected for an underestimate of internal bremsstrahlung. In both cases, the charged particles are corrected for external bremsstrahlung. Finally, the resulting e^+ and e^- vectors are smeared according to the measurement resolutions in momentum and production angles.

1. *Soft-photon correction for the elastic events*

The α^3 QED calculation suppresses soft photons having $k/E_{\text{beam}} < 0.01$, so that all events with photon energies below this limit are generated as elastic events. This suppression does not affect the cross section, but does cause a minor problem with the theoretical acollinearity distribution. The soft photons have been restored by the following empirical procedure. First, a photon energy is chosen according to the distribution:

$$\begin{aligned} dN/dk &= \text{const} \quad \text{for } 0 < k/E_{\text{beam}} < a \\ &= \text{const}(aE_{\text{beam}}/k) \quad \text{for } a < k/E_{\text{beam}} < 0.01 , \end{aligned} \tag{10}$$

where a is a constant ($=0.0042$) chosen to preserve the normalization. The photon parent is randomly chosen from among the four possibilities of incoming or outgoing, e^+ or e^-. Next, the photon direction with respect to the parent axis is distributed according to

$$dN/d\cos\beta = \text{const}/[1-\cos\beta+(m_e/E_{\text{beam}})^2/2] , \tag{11}$$

where β is the angle between the photon and parent, and m_e is the mass of the electron. Finally, the momenta of the outgoing charged particles are adjusted to conserve energy and momentum.

2. *Bremsstrahlung*

Bremsstrahlung causes a shift of the electron momentum spectrum to lower values than expected on the basis of the α^3 QED calculation. This effect will occasionally reduce the electron momentum sufficiently that it falls below the momentum cutoff of 7.5 GeV/c. The bremsstrahlung correction consists of an external part and an internal part.

The mean material thickness contributing to external bremsstrahlung in the HRS, t_{eff}, is 0.017 ± 0.002 r.l. This includes 35% of the gas thickness in the central drift chamber and a correction for the average polar angle of the electron tracks. A good approximation[20] for the probability that an electron with an initial energy E_0 will pass through a thin radiator and emerge with an energy in the interval from $E-\Delta E/2$ to $E+\Delta E/2$ is

$$P(E_0,E,\Delta E) = t_{\text{eff}}\{\tfrac{4}{3}\ln[(E_0-E+\Delta E/2)/(E_0-E-\Delta E/2)] - \Delta E/3E_0 - E\Delta E/E_0^2\} . \tag{12}$$

For each e^- or e^+ particle generated by the Berends and Kleiss program, a value of E/E_0 is randomly chosen according to this distribution. If $E/E_0 < 0.99$, then E_0 is replaced by E, thereby shifting a portion of the momentum distribution to lower values.

The events generated by the Berends-Kleiss program allow radiation to occur either in the initial state or in the final state, but not in both. The final-state radiation is similar to bremsstrahlung because it is emitted with a $(1/k)$-like energy spectrum along the direction of a parent electron; thus this radiation is sometimes called internal bremsstrahlung. If a generated event undergoes initial-state radiation, then the Berends-Kleiss calculation, by construction, allows no final-state radiation. Therefore the α^3 QED calculation yields a momentum spectrum that shows less internal bremsstrahlung than is physically

produced.

An empirical correction has been made for this omitted internal bremsstrahlung. Each generated nonelastic event is examined to see if the photon appears to have been produced by initial-state radiation along the direction of the incident e^- or e^+. If the event has an initial-state radiation, then 50% of the time there will have been no opportunity, within the Berends-Kleiss program, to permit internal bremsstrahlung. This omission is corrected by allowing a random 50% of such events to have one electron that radiates according to a probability function similar to that in Eq. (12). This extra contribution to internal bremsstrahlung only affects the α^3 QED calculation indirectly through the momentum cut. The internal bremsstrahlung correction is done prior to the external bremsstrahlung correction.

3. *Momentum smearing for electrons*

After the above corrections are made, the electron vectors are smeared according to the detector resolutions for momentum and production angles listed in Table I. The variables smeared are θ, ϕ, and p_T, the momentum transverse to the beam direction. To a good approximation, these variables are independent, so they are smeared without correlations.

A careful study of the angular distributions revealed a small misalignment of the drift-chamber stereo layers, such that tracks were reconstructed with θ shifted by an average of 1.5 mrad from the true direction. This small shift is added to the simulated events at this stage.

The momentum smearing is done by adding in quadrature the effects of setting error and multiple scattering. The setting error is dominant for tracks above 5 GeV/c. For the final sample of Bhabha events, 38% of the e^+ and e^- tracks were reconstructed using the central drift chamber only. The smearing program accounts for this effect on a random basis by using the larger setting error for this fraction of tracks.

C. Experiment simulation for γ-pair production

The detector simulation of photon showers for generated γ-pair events is done in three steps.

(a) Photons striking the calorimeter within $\pm 0.24°$ of the azimuthal boundary between modules are omitted. This step closely imitates the signal loss at the walls. The value of 0.24° reproduces the observed 5.9% event loss

TABLE XII. Differential cross sections for Bhabha scattering at 29 GeV. The scattering angles of both tracks are used, each with weight 0.5. The quoted uncertainties are mainly statistical, but include small systematic contributions from acceptance uncertainties. An overall systematic uncertainty of 0.9% is not included.

	Number of events		Ratio			$s\left[\frac{d\sigma}{d\Omega}\right]$		$s\left[\frac{d\sigma^e}{d\Omega}\right]_{GSW}$
$\cos\theta$	Observed	Expected	$\left[\frac{\text{observed}}{\text{expected}}\right]$	A[a]	$(1+\delta_{QED})$[b]	(GeV^{2}nb/sr)	$(1+\delta_{GSW})$[a]	(GeV^{2}nb/sr)
−0.525	1064.5	1095.8	0.971±0.041	0.833	0.911	22.8±1.0	0.984	23.5
−0.475	1306.0	1275.3	1.024±0.033	0.933	0.914	24.9±0.8	0.982	24.4
−0.425	1346.0	1373.3	0.980±0.028	0.967	0.913	24.8±0.7	0.981	25.3
−0.375	1360.5	1453.3	0.936±0.025	0.978	0.913	24.7±0.7	0.980	26.5
−0.325	1476.0	1530.5	0.964±0.025	0.979	0.913	26.8±0.7	0.979	27.9
−0.275	1619.5	1620.7	0.999±0.025	0.979	0.913	29.4±0.7	0.979	29.5
−0.225	1733.0	1727.9	1.003±0.024	0.979	0.913	31.5±0.8	0.979	31.5
−0.175	1834.0	1853.6	0.989±0.023	0.979	0.913	33.3±0.8	0.979	33.8
−0.125	1982.5	2003.8	0.989±0.022	0.979	0.913	36.0±0.8	0.980	36.5
−0.075	2132.5	2182.6	0.977±0.021	0.979	0.913	38.7±0.8	0.981	39.7
−0.025	2418.5	2396.4	1.009±0.021	0.979	0.914	43.9±0.9	0.982	43.6
0.025	2630.0	2649.7	0.993±0.019	0.979	0.913	47.8±0.9	0.983	48.3
0.075	2987.5	2960.7	1.009±0.018	0.979	0.913	54.3±1.0	0.985	53.9
0.125	3429.5	3335.1	1.028±0.018	0.979	0.913	62.3±1.1	0.987	60.8
0.175	3802.5	3796.4	1.002±0.016	0.979	0.913	69.1±1.1	0.989	69.2
0.225	4320.0	4372.2	0.988±0.015	0.979	0.914	78.4±1.2	0.990	79.6
0.275	5056.0	5101.1	0.991±0.014	0.979	0.916	91.6±1.3	0.992	92.6
0.325	6186.5	6027.2	1.026±0.013	0.979	0.919	111.7±1.4	0.994	109.1
0.375	7122.5	7216.7	0.987±0.012	0.977	0.922	128.4±1.5	0.996	130.4
0.425	8558.0	8630.9	0.992±0.011	0.961	0.924	156.5±1.8	0.997	158.2
0.475	10363.0	10385.2	0.998±0.011	0.933	0.927	194.6±2.2	0.999	195.5
0.525	11694.5	11471.6	1.019±0.013	0.814	0.930	250.8±3.3	1.000	246.6

[a] A is the angular acceptance, including event losses at the azimuthal walls between calorimeter modules and losses from the fiducial cut.

[b] Radiative correction to order α^3, including the effects of cuts on acollinearity and momentum.

[c] Expected electroweak correction at 29 GeV.

(see Table X).

(b) If the event has three photons, and if two of them strike neighboring barrel modules, then the two are merged into one shower. This is a reasonable approximation to the experimental situation. This merger is applied to only a small percentage of events.

(c) The photon variables are then smeared according to the resolutions for shower energies and positions. A small fraction (4.3%) of the observed photons convert beyond the PWC plane. The same fraction of simulated photons are picked at random and treated as if they have no PWC information; for such photons, ϕ is set to the center of the module and θ is smeared with a resolution given by the timing measurements.

VI. RESULTS

A. Luminosity measurements

The Berends-Kleiss programs provide calculated cross sections summed over a certain phase space of an ideal detector. The Monte Carlo events are corrected and smeared according to the real detector conditions, as just discussed, and then subjected to the same selections as are applied to the data. This procedure yields the α^3 QED cross sections corresponding to the resolution and acceptance of the experiment. The integrated luminosity of the data sample is then found from the number of observed events divided by this cross section.

For Bhabha scattering, the α^3 QED cross section for the conditions imposed by the experiment is 529.3 pb. If the electroweak corrections are included, then the cross section is reduced by 0.96%. Since the corrected number of observed events is 86 190, the measured integrated luminosity is 164.4 pb^{-1}. For γ-pair production, the α^3 QED cross section for the conditions imposed by the experiment is 95.7 pb, and the corrected number of observed events is 15 850, so the integrated luminosity is 165.6 pb^{-1}. The weighted average of these two numbers is 164.8 pb^{-1}, as given in Table IV.

B. Differential cross sections for Bhabha scattering

The measured differential cross section for Bhabha scattering at 29 GeV in the central polar angle region, $|\cos\theta| < 0.55$, is given in Table XII, where the normalization is 164.8 pb^{-1}. These numbers have also been corrected for electroweak effects. That is,

$$N_{\mathrm{GSW}}(\cos\theta) = N_{\mathrm{QED}}(\cos\theta)(1+\delta_{\mathrm{GSW}}) \, . \tag{13}$$

The electroweak correction is obtained from the ratio of

TABLE XIII. Differential cross sections for $e^+e^- \to \gamma\gamma$ at 29 GeV. Both photons are used, each with a weight 0.5. The quoted uncertainties are mainly statistical but include small systematic contributions from acceptance uncertainties. An overall systematic uncertainty of 0.9% is not included.

	Number of events		Ratio			$s\left[\frac{d\sigma}{d\Omega}\right]$	$s\left[\frac{d\sigma^\circ}{d\Omega}\right]_{\mathrm{QED}}$
$\lvert\cos\theta\rvert$	Observed	Expected	$\left[\frac{\text{observed}}{\text{expected}}\right]$	A[a]	$(1+\delta_{\mathrm{QED}})$[b]	($\mathrm{GeV^2nb/sr}$)	($\mathrm{GeV^2nb/sr}$)
0.0125	558.5	552.9	1.010±0.043	0.939	0.922	21.0±0.9	20.7
0.0375	549.0	554.2	0.991±0.042	0.939	0.922	20.6±0.9	20.8
0.0625	539.0	557.0	0.968±0.042	0.939	0.922	20.2±0.9	20.9
0.0875	539.0	561.2	0.960±0.041	0.939	0.922	20.2±0.9	21.1
0.1125	567.0	566.9	1.000±0.042	0.939	0.922	21.3±0.9	21.3
0.1375	570.5	573.9	0.994±0.042	0.939	0.922	21.4±0.9	21.5
0.1625	576.0	582.6	0.989±0.041	0.939	0.922	21.6±0.9	21.9
0.1875	574.0	593.0	0.968±0.040	0.939	0.922	21.5±0.9	22.3
0.2125	596.0	605.0	0.985±0.040	0.939	0.922	22.4±0.9	22.7
0.2375	605.0	618.7	0.978±0.040	0.939	0.922	22.7±0.9	23.2
0.2625	625.0	634.5	0.985±0.039	0.939	0.922	23.5±0.9	23.8
0.2875	650.5	652.3	0.997±0.039	0.939	0.922	24.4±1.0	24.5
0.3125	635.5	672.3	0.945±0.037	0.939	0.922	23.8±0.9	25.2
0.3375	706.5	694.7	1.017±0.038	0.939	0.922	26.5±1.0	26.1
0.3625	744.0	719.5	1.034±0.038	0.939	0.922	27.9±1.0	27.0
0.3875	742.5	745.9	0.995±0.037	0.935	0.923	27.9±1.0	28.1
0.4125	797.5	774.4	1.030±0.037	0.928	0.927	30.1±1.1	29.2
0.4375	872.5	803.6	1.086±0.038	0.919	0.929	33.2±1.2	30.6
0.4625	846.0	833.3	1.015±0.036	0.906	0.933	32.5±1.2	32.0
0.4875	858.5	863.7	0.994±0.036	0.892	0.934	33.5±1.2	33.7
0.5125	921.5	876.6	1.051±0.038	0.864	0.928	37.3±1.3	35.5
0.5375	800.0	778.2	1.028±0.042	0.723	0.930	38.6±1.6	37.6

[a] A is the angular acceptance, including event losses at the azimuthal walls between calorimeter modules and losses from the fiducial cut.

[b] Radiative correction to order α^3, including the effects of the acollinearity cut.

second-order differential cross sections

$$(1+\delta_{\rm GSW})=(d\sigma^0_{ee}/d\Omega)_{\rm GSW}/(d\sigma^0_{ee}/d\Omega)_{\rm QED}\ , \qquad (14)$$

where the second-order expressions are evaluated analytically using Eqs. (3)–(5). The numerical values for this correction are also listed in Table XII.

The ratio of measured to predicted differential cross sections, fully corrected for event selections, experimental acceptance, and resolutions, provides the final comparison between the measurements of Bhabha scattering and α^3 QED theory.

The absolute differential cross section for Bhabha scattering, corrected for α^3 effects, may be compared to the theoretical result to second order, including electroweak contributions. The experimental values are given by

$$s(d\sigma/d\Omega)_i=(s/L\,\Delta\Omega)(N_i/A_i)/(1+\delta_{\rm QED})_i\ , \qquad (15)$$

where L is the integrated luminosity of the sample, $\Delta\Omega$ the solid angle of the bin, N_i the number of observed events in the ith bin, A_i the angular acceptance factor, and $(1+\delta_{\rm QED})_i$ the α^3 radiative correction. The factor A_i includes both the azimuthal loss at the barrel walls and the loss caused by imposing the fiducial cut at $|\cos\theta|=0.55$. The radiative correction includes the effects of the momentum and acollinearity cuts, but is independent of the angular acceptance. Both A_i and $(1+\delta_{\rm QED})_i$ are determined by comparing the results of the full Monte Carlo calculation to a second Monte Carlo calculation for an HRS-like detector having 4π sr solid-angle acceptance.

C. Differential cross sections for γ-pair production

The measured differential cross section for γ-pair production at 29 GeV in the central polar-angle region, $|\cos\theta|<0.55$, is given in Table XIII, where the normalization is 164.8 pb^{-1}.

The meaning of the various columns in Table XIII is the same as for Table XII, except that there are no electroweak contributions for this reaction. The distribution is given for only one hemisphere, since the final-state photons are indistinguishable.

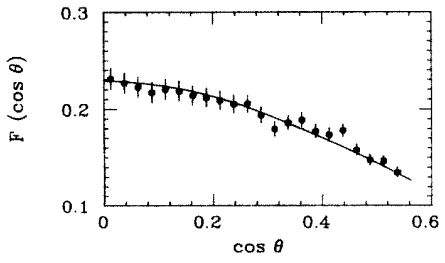

FIG. 15. Ratio of the γ-pair differential cross section to the Bhabha differential cross section at 29 GeV. In determining this ratio, denoted by $F(\cos\theta)$, the Bhabha spectrum has been folded at $\cos\theta=0$. The curve shows the prediction of QED to order α^3 together with a small ($\sim$1%) correction for known electroweak contributions.

D. Comparison of experiment to α^3 QED theory

Figure 15 displays a bin-by-bin comparison of the differential cross sections for the two reactions, where

$$F(\cos\theta)=N_{\gamma\gamma}(\cos\theta)/[N_{ee}(\cos\theta)+N_{ee}(-\cos\theta)]\ , \qquad (16)$$

and where $N_{\gamma\gamma}$ and N_{ee} are the observed numbers of events from Tables XII and XIII. The uncertainties shown in Fig. 15 are statistical. The curve shows the expected α^3 QED result, including the small electroweak contribution to Bhabha scattering. The agreement between theory and experiment is excellent over the whole region, yielding $\chi^2=15.9$ for 22 degrees of freedom. A comparison of the entire data sample to theory gives

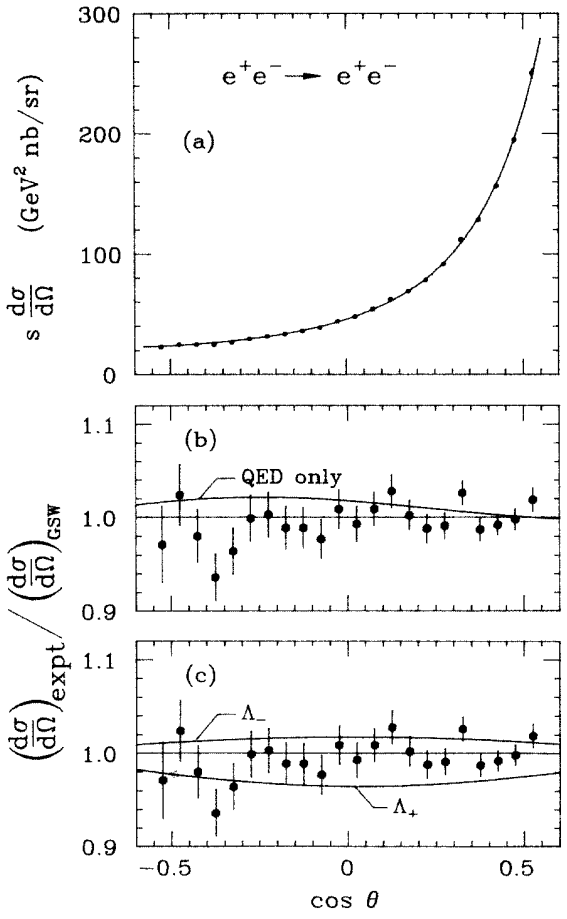

FIG. 16. (a) Bhabha differential cross section at 29 GeV. The data points have been adjusted in this plot to remove acceptance losses and to remove the calculated α^3 QED effects. The curve is the second-order QED prediction together with the electroweak contribution. (b) Ratio of the observed differential distribution to that from the full Monte Carlo simulation of the experiment, including α^3 QED and electroweak contributions. For comparison, the curve shows the pure QED result (with $g_A{}^2=g_V{}^2=0$). (c) The same ratio as in (b) compared to the lower bounds (at 95% confidence) of the QED-cutoff parameters, Λ_+ and Λ_-.

TABLE XIV. Comparison of QED-cutoff parameters. The values given are 95% confidence lower limits on the cutoff parameters.

		$e^+e^- \to e^+e^-$		$e^+e^- \to \gamma\gamma$	
Experiment	Reference	Λ_+ (GeV)	Λ_- (GeV)	Λ_+ (GeV)	Λ_- (GeV)
CELLO	6	74	150	59	44
JADE	3	178	200	61	57
Mark J	2	165	235	72	
PLUTO	5	184	162		
TASSO	7	151	251	61	56
HRS	This expt.	154	220	59	59

$$\frac{\Sigma(\text{expt})}{\Sigma(\text{QED})} = 1.007 \pm 0.009 \pm 0.008 \pm \delta(\alpha^3) , \quad (17)$$

where Σ is the integral of $F(\cos\theta)$ over $|\cos\theta| < 0.55$. The first uncertainty is statistical, the second is systematic, and the term $\delta(\alpha^3)$ represents the uncertainty in the ratio of the theoretical cross sections calculated to this order. The value of $\delta(\alpha^3)$ is not known, but is estimated to be approximately 1% (Ref. 22). The theoretical uncertainty in the electroweak correction for Bhabha scattering at 29 GeV is negligible compared to $\delta(\alpha^3)$. The overall experimental accuracy of this comparison is 1.2% if the statistical and systematic uncertainties are added in quadrature, or 1.7% if they are added linearly.

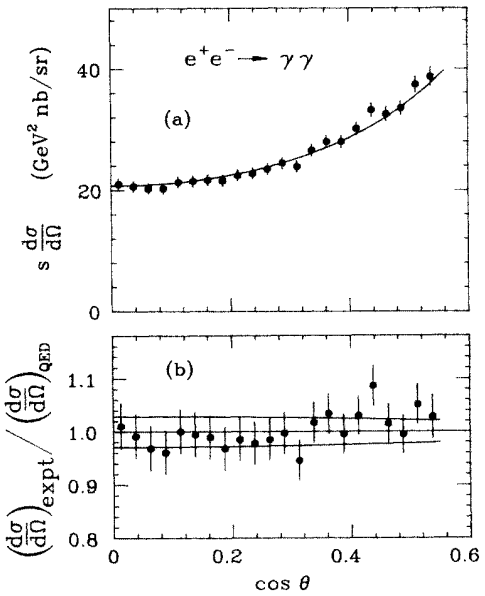

FIG. 17. (a) γ-pair differential cross section at 29 GeV. The data points have been adjusted in this plot to remove acceptance losses and to remove the calculated α^3 QED effects. The curve is the second-order QED prediction. (b) Ratio of the observed differential distribution to that from the full Monte Carlo simulation of the experiment, including α^3 QED contributions. The upper and lower curves, respectively, represent the lower bounds (at 95% confidence) of the QED-cutoff parameters, Λ_+ and Λ_-.

The differential cross section for Bhabha scattering is displayed in Fig. 16(a), where it is compared to the second-order theory with the electroweak correction included. This comparison is shown in more detail in Fig. 16(b), which displays the ratio of the differential cross sections. The curve in 16(b) is the result of theory with the electroweak correction turned off. The agreement between the experiment and the GSW calculation is excellent, giving $\chi^2 = 23.8$ for 22 degrees of freedom. On the other hand, the pure-QED curve provides a relatively poor fit with $\chi^2 = 35.4$.

The 95%-confidence limits for the Bhabha QED-cutoff parameters are $\Lambda_+ > 154$ GeV and $\Lambda_- > 220$ GeV. In determining these limits, the uncertainty of the integrated luminosity has been taken into account.[14] Figure 16(c) shows curves corresponding to these limits. A value of $\Lambda = 200$ GeV implies pointlike scattering down to a distance of 10^{-18} m. The limits reported at higher energies by the PETRA experiments are similar to the present results, as is summarized in Table XIV.

The differential cross section for γ-pair production is shown in Fig. 17(a); the curve is from the second-order theory. The same comparison is displayed in Fig. 17(b) as the ratio of differential cross sections, where the upper and lower curves are the 95%-confidence limits for the QED-cutoff parameters, $\Lambda_+ > 59$ GeV and $\Lambda_- > 59$ GeV. Again, the uncertainty of the integrated luminosity has been taken into account in finding these limits. The value of Λ_+ may be interpreted as a lower limit on the mass of a heavy electron that could be exchanged in this reaction. Other experiments at higher energy have found comparable limits on the QED-cutoff parameters.

VII. SUMMARY

A major part of this paper has discussed the methods of analysis in some detail in order to validate the quoted systematic accuracy. The present experiment demonstrates that, in comparing the ratio of the differential cross sections for Bhabha scattering and γ-pair production, the predictions of α^3 QED are valid to within an accuracy of 2% or better. This is the most rigorous test of QED reported at PEP or PETRA energies, as the competing ex-

periments have reported systematic uncertainties in the range 3–6% arising from luminosity measurements or inefficiencies in event identification procedures.

The two reactions have been used to determine lower limits on the QED-cutoff parameters. The sensitivity in setting these limits is proportional to s for Bhabha scattering and to s^2 in γ-pair production, so there is a significant advantage in carrying out these studies at the highest energy available. The present work at 29 GeV has founds limits comparable to those from the PETRA experiments done above 34 GeV. This has been achieved by analyzing more wide-angle events and by a careful control of systematic effects.

ACKNOWLEDGMENTS

This work has been made possible by the outstanding support of the technical staffs at SLAC and the collaborating institutions. Special thanks are due to J. Nolan and B. Martin for their steady efforts throughout the construction and operation of the HRS facility, E. Patterson and the PEP operations staff, R. Watt and the cryogenics group, and J. Brown and the VAX computer group. This work was supported in part by the U.S. Department of Energy, under Contracts Nos. W-31-109-ENG-38, DE-AC02-7ER01112, DE-AC03-76SF00098, DE-AC02-76ER01428, and DE-AC02-84ER40125.

---

[a]Present address: Stanford Linear Accelerator Center, Stanford, CA 94305.
[b]Present address: AT&T Bell Laboratories, Naperville, IL 60566.
[c]Present address: SRI International, Menlo Park, CA 94025.
[d]Present address: Lockheed Missiles and Space Co., Sunnyvale, CA 94086.
[e]Present address: Laboratory for Nuclear Studies, Cornell University, Ithaca, NY 14853.
[f]Permanent address: INFN, Pisa, Italy.
[g]Present address: CERN, 1211 Geneva 23, Switzerland.
[h]Present address: Brandeis University, Waltham, MA 02254.
[i]Present address: ETH, Zurich, Switzerland.

[1]HRS Collaboration, D. Bender *et al.*, Phys. Rev. D **30**, 515 (1984).
[2]Mark J. Collaboration, B. Adeva *et al.*, Phys. Lett. **152B**, 439 (1985); Phys. Rev. Lett. **53**, 134 (1984).
[3]JADE Collaboration, W. Bartel *et al.*, Z. Phys. C **19**, 197 (1983).
[4]Mark II Collaboration, M. E. Levi *et al.*, Phys. Rev. Lett. **51**, 1941 (1983).
[5]PLUTO Collaboration, Ch. Berger *et al.*, Z. Phys. C **27**, 341 (1985).
[6]CELLO Collaboration, H.-J. Behrend *et al.*, Phys. Lett. **140B**, 130 (1984); **123B**, 127 (1983); Z. Phys. C **16**, 301 (1983).
[7]TASSO Collaboration, M. Althoff *et al.*, Phys. Lett. **154B**, 236 (1985); Z. Phys. C **22**, 13 (1984); **26**, 337 (1984).
[8]S. L. Glashow, Nucl. Phys. **22**, 579 (1961); A. Salam and J. C. Ward, Phys. Lett. **13**, 168 (1964); S. Weinberg, Phys. Rev. Lett. **19**, 1264 (1967); Phys. Rev. D **5**, 1412 (1972).
[9]S. D. Drell, Ann. Phys. (N.Y.) **4**, 75 (1958).
[10]A. Litke, Ph.D. thesis, Harvard University, 1970.
[11]E. J. Eichten, K. D. Lane, and M. E. Peskin, Phys. Rev. Lett. **50**, 811 (1983).
[12]W. Hollik, F. Schrempp, and B. Schrempp, Phys. Lett. **140B**, 424 (1984); R. D. Pecci, *ibid.* **136B**, 121 (1984); F. M. Renard, *ibid.* **139B**, 449 (1984); F. W. Bopp *et al.*, Z. Phys. C **24**, 367 (1984).
[13]The theoretical QED calculations to order α^3 are done by means of Monte Carlo event-generating programs that are based on methods outlined in F. A. Berends and R. Kleiss, Nucl. Phys. **B228**, 537 (1983); **B186**, 22 (1981). These authors have made their programs available to the experimental community.
[14]HRS Collaboration, M. Derrick *et al.*, Phys. Lett. **166B**, 463 (1986); **166B**, 468 (1986).
[15]Throughout this paper, the following values are used for the electroweak parameters: $M_Z = 93$ GeV/c^2, $g_A{}^2 = 0.25$, and $g_V{}^2 = 0.004$. These values are based on Refs. 16 and 17.
[16]W. J. Marciano and S. Sirlin, Phys. Rev. D **29**, 945 (1984).
[17]UA2 Collaboration, M. Bagnaia *et al.*, Phys. Lett. **129B**, 130 (1983); UA1 Collaborarion, G. Arnison *et al.*, *ibid.* **147B**, 241 (1984).
[18]G. Baranko *et al.*, Nucl. Instrum. Methods **169**, 413 (1980); D. Rubin *et al.*, *ibid.* **203**, 119 (1982).
[19]J. S. Loos *et al.*, Nucl. Instrum. Methods **A249**, 185 (1986).
[20]B. Rossi, *High Energy Physics* (Prentice-Hall, New York, 1952).
[21]M. Derrick *et al.*, Phys. Rev. D **34**, 3304 (1986).
[22]Y. S. Tsai, SLAC Report No. SLAC-PUB-3129, 1983 (unpublished); MAC Collaboration, E. Fernandez *et al.*, Phys. Rev. D **31**, 1537 (1985).